Journal of Ceramic Processing Research. Vol. 21, No. 6, pp. 699~704 (2020)
(Received 22 July 2020, Received in revised form 17 October 2020, Accepted 23 October 2020)
https://doi.org/10.36410/jcpr.2020.21.6.699

J O U R N A L O F
Ceramic Processing Research

Tetrasodium iminodisuccinate assisted hydrothermal synthesis and upconversion luminescence of $NaYF_4$: Yb^{3+}, Er^{3+} hexagonal nanoplates

Haiyan Lin[#], Zikun Wang[#], Yujiang Wang and Junwei Zhao*
Materials Science and Engineering School & Henan Key Laboratory of Special Protective Materials, Luoyang Institute of Science and Technology, Luoyang, 471023, P. R. China

Yb^{3+}/Er^{3+} co-doped $NaYF_4$ ($NaYF_4$: Yb^{3+}, Er^{3+}) hexagonal nanoplates were synthesized by a tetrasodium iminodisuccinate assisted hydrothermal synthesis method for the first time. The crystal structure and morphology was investigated by the X-ray diffraction and scanning electron microscope analysis. The upconversion luminescent property of the synthesized $NaYF_4$: Yb^{3+}, Er^{3+} hexagonal nanoplates was discussed as a function of Yb^{3+} and Er^{3+} concentration. Under 980 nm excitation, $NaYF_4$: Yb^{3+}, Er^{3+} hexagonal nanoplates exhibited strong red emissions near 660 nm and green upconversion emissions at 530 and 550 nm corresponding to the intra 4f transitions of Er^{3+} ($^4F_{9/2}$, $^2H_{11/2}$, $^4S_{3/2}$) → Er^{3+} ($^4I_{15/2}$). The Yb^{3+} 5 mol% and Er^{3+} 0.5 mol% co-doped $NaYF_4$ sample exhibited strongly shiny upconversion emission, which was considered to be the optimum doping concentration. A possible upconversion mechanism for $NaYF_4$: Yb^{3+}, Er^{3+} depending was discussed in detail.

Keywords: hydrothermal, $NaYF_4$, upconversion, IDS.

Introduction

In the past decades, upconversion luminescent (UCL) nanomaterials doped with rare earth ions have become one of the research focuses in the field of materials and luminescence [1-12]. UCL nanomaterials have potential promising applications in many fields, such as optical communication, luminescence display, high density storage, infrared detection and biomedical imaging [13-15]. Up to now, rare earth ions have been doped in many matrix materials and UCL has been successfully realized [16]. The transition of electrons in the 4f shell of rare earth ions induces narrow band luminescence, which are very sensitive to the composition and crystal structure of the matrix materials [1, 10, 16]. Er^{3+} has been considered to be an ideal doping ion to realize infrared to visible UCL owing to its good matching energy level and long excited state lifetime [17]. Compared with Er^{3+}, Yb^{3+} has a larger optical absorption cross section in the infrared wavelength, which can effectively transfer the absorbed light energy to Er^{3+} [18, 19]. Therefore, as a sensitizer, Yb^{3+} can effectively increase the emission efficiency of the luminescence center [20-24]. Rare earth ions are easy to cause multiphonon relaxation due to their abundant energy levels and small energy gap between energy levels [25]. Therefore, materials with relatively low phonon energy being used as the matrix can effectively reduce the luminescence loss caused by the non-radiative process [9]. This is particularly important for the upconversion process, which is related to the fluorescence quenching because of high energy vibration. The phonon energy of fluoride is much lower than that of oxide. The multiphonon relaxation of rare earth ions can be reduced by using fluoride as matrix material [9]. Among them, the rare earth ion UCL materials based on $NaYF_4$ are found to be of high efficiency in recent years [1, 25, 26].

In the past years, there have been many reports on upconversion materials based on $NaYF_4$ [9]. In order to effectively control the nucleation and growth process of nanocrystals by wet chemical method, it is often necessary to introduce organic reagents as ligands or chelators in the synthesis process [27, 28]. In this paper, $NaYF_4$: Yb^{3+}, Er^{3+} hexagonal nanoplates with UCL were prepared by coprecipitation and hydrothermal method using tetrasodium iminodisuccinate (IDS Na_4) as chelating agent and NaF as precipitant. The influence of Yb^{3+} and Er^{3+} concentration on the upconversion luminescence of $NaYF_4$: Yb^{3+}, Er^{3+} hexagonal nanoplates was studied in detail. A possible upconversion mechanism for $NaYF_4$: Yb^{3+}, Er^{3+} hexagonal nanoplates was proposed. The results provide new insights for the research of other upconversion luminescent materials.

Experimental

Firstly, the rare earth nitrate mixed aqueous solution (molar ratio, Y: Yb: Er = 89 : 10 : 1, 10 mL, 0.1 mol/L)

[#]These authors contributed equally.
*Corresponding author:
Tel : +86-379-65928196
Fax: +86-379-65928196
E-mail: jwzhao2010@lit.edu.cn

was added into an IDS Na_4 aqueous solution (10 mL, 0.1 mol/L) under magnetic stirring, and the reaction lasted for half an hour to obtain the chelate complex of rare earth ions and IDS Na_4. Then the NaF aqueous solution (20 mL, 0.4 mol/L) was injected into the above reaction system, and the reaction lasted for one hour to obtain the precursor solution. After that, the reactant solution was transferred to a hydrothermal reactor, and the hydrothermal reaction was performed at 180 ºC for 15 h. The obtained samples were centrifuged at 3,500 rpm for 15 min, and the precipitates were retained. Finally, the samples were dried in an oven at 60 ºC for 24 h to obtain the final products. The synthesis process of other doping concentrations is similar.

The crystal structure was characterized by X-ray diffraction (XRD, Y-4Q, CuKα, λ = 1.5418 Å). The morphology and particle size of the products were observed by scanning electron microscope (SEM, FEI Quanta 250 FEG). UCL spectra were measured in the range of 500-800 nm using a photoluminescence spectrophotometer (PerkinElmer, LS55) with a semiconductor laser diode (980 nm, 3W) as an external excitation source.

Results and Discussion

The synthesis process of $NaYF_4$:Yb, Er phosphors is illustrated in Fig. 1. In our case, the chelate complex of rare earth ions and IDS Na_4 (Ln-IDS) was formed at the beginning. After the addition of NaF aqueous solution, the F^- anion must compete with the chelating agent to transform the Ln-IDS complex into the $NaYF_4$ lattice. Fig. 2 shows the representative XRD pattern of $NaYF_4$: Yb^{3+}, Er^{3+} phosphors. As shown in Fig. 2, the XRD peaks were in accordance with that of hexagonal β-$NaYF_4$ (JCPDF card 28-1192) [17, 28]. There are no diffraction peaks corresponding to impurities of α-NaYF4 (JCPDS card 77-2042), indicating the high purity of the as-obtained products. The XRD pattern of the sample shows clear and sharp peaks, which indicate the high crystallinity of the obtained product.

Fig. 3 shows the representative SEM images of $NaYF_4$: Yb^{3+}, Er^{3+} phosphors with different magnifications. It is observed that the obtained $NaYF_4$: Yb^{3+}, Er^{3+} phosphors are uniform and monodisperse hexagonal nanoplates. The size is about 500 nm × 220 nm (side length × thickness). In our previous work, we prepared similar $NaYF_4$: Yb^{3+}, Er^{3+} hexagonal nanoplates with trisodium citrate as chelating agent [28]. It is one of the basic deposition processes that chelating agent (e.g. ethylene diamine tetraacetic acid disodium salt and trisodium citrate) controls the nucleation and growth of inorganic structures [27, 28]. In our present case, we used IDS Na_4 as chelating agent and obtained similar

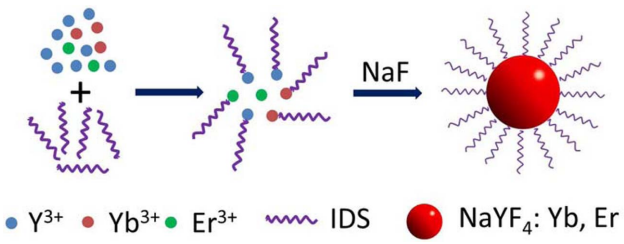

Fig. 1. Schematic illustration of the synthesis process of $NaYF_4$:Yb, Er.

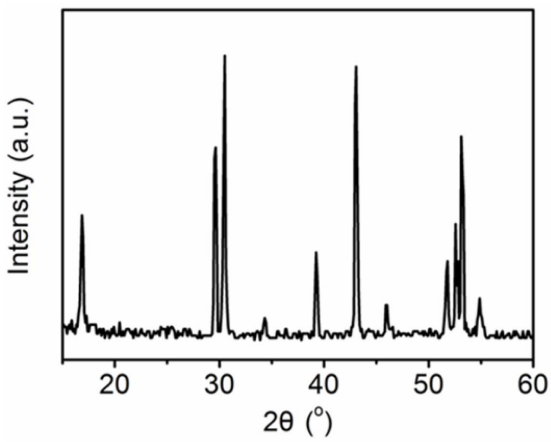

Fig. 2. The representative XRD pattern of $NaYF_4$: Yb^{3+}, Er^{3+} phosphors.

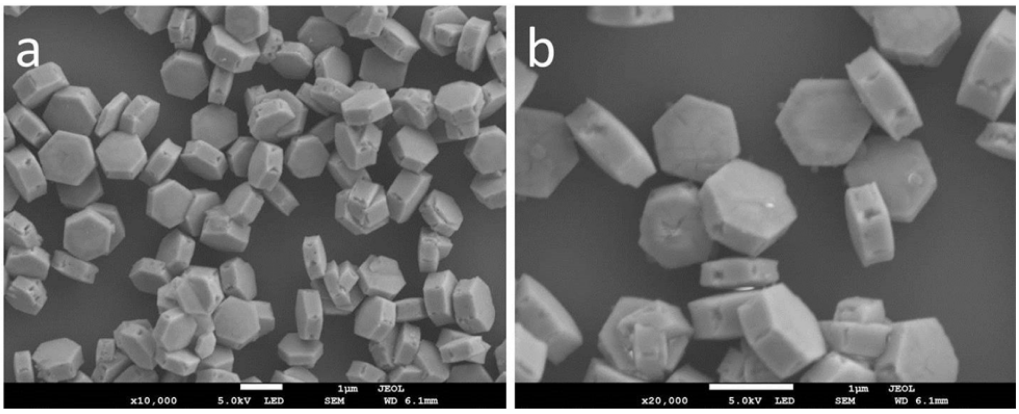

Fig. 3. The representative SEM images of $NaYF_4$: Yb^{3+}, Er^{3+} phosphors with different magnifications.

results. IDS Na_4 is a biodegradable chelating agent, and its chelating capacity can comparable with that of ethylene diamine tetraacetic acid. Chelating agents coordinate with metal ions in the synthesis process through amine, carboxyl group, hydroxyl and other functional groups, and passivate the surface of nanoparticles after synthesis, which are effective ligands of the synthesis of inorganic nanomaterials [27, 28]. In this study, IDS Na_4 and rare earth nitrate were incubated under environmental conditions to form the coordination between Ln^{3+} and IDS Na_4 and promote heterogeneous nucleation. Then, the freshly prepared NaF solution was injected into the mixed solution with vigorous stirring. The mixture underwent hydrothermal crystallization, and finally $NaYF_4$: Yb^{3+}, Er^{3+} hexagonal nanoplates were obtained. In addition, IDS Na_4 molecules were coated on $NaYF_4$: Yb^{3+}, Er^{3+} to make the products water-soluble and biocompatible.

Fig. 4(a) shows the UCL spectra of representative $NaYF_4$: Yb^{3+} 5%, Er^{3+} 0.5% hexagonal nanoplates excited by a 980 nm near-infrared laser. The $NaYF_4$: Yb^{3+} 5%, Er^{3+} 0.5% hexagonal nanoplates exhibit UCL from infrared to visible emission. The visible emission bands are around at 530 nm and 550 nm, which originate from the transition of electrons from $^2H_{11/2}$ and $^4S_{3/2}$ to $^4I_{15/2}$ in Er^{3+} ions. The emission band near 660 nm is attributed to the transition of $^4F_{9/2}$ level to $^4I_{15/2}$ level in Er^{3+} ions. The emission intensities of green and red bands of the $NaYF_4$: Yb^{3+} 5%, Er^{3+} 0.5% hexagonal nanoplates increase gradually with the increase of the laser excitation power. To understand the UCL process and the population of $^2H_{11/2}$, $^4S_{3/2}$ and $^4F_{9/2}$ excited states under infrared wavelength excitation, it is necessary to study the relationship between laser excitation power and UCL intensity. The upconversion process involves multiphoton absorption, and there is a relationship between the intensity of the output visible light and the excitation power:

$$I_{VIS} \propto P_{IR}{}^{n} \quad (1)$$

where I_{VIS} is the intensity of visible upconversion emission, I_{IR} is the excitation power, and n is the number of infrared photons needed to be absorbed by the sample to emit a visible photon. Fig. 4(b) shows the excitation power relationship of the UCL spectra of the $NaYF_4$: Yb^{3+} 5%, Er^{3+} 0.5% hexagonal nanoplates. The emission intensity increases with the increase of excitation power density. The slopes of ($^2H_{11/2}$, $^4S_{3/2}$) $\rightarrow{}^4I_{15/2}$ and $^4F_{9/2}\rightarrow{}^4I_{15/2}$ transitions are 1.57 and 1.50, respectively. It is shown that UCL involves a two-photon absorption process (Fig. 5) [28, 29]. The slopes deviate from 2 because of the competition between different decay channels in the intermediate state. These decay channels include multiphonon relaxation of low energy state, radiation decay of ground state, upconversion of intermediate state and non-radiation capture [30].

To study the effect of Er^{3+} concentration on UCL in $NaYF_4$: Yb^{3+}, Er^{3+} hexagonal nanoplates and to explore the optimum doping concentration of Er^{3+}, a series of powder samples of $NaYF_4$: Yb^{3+} 10%, Er^{3+} x% doped with Er^{3+} of different concentrations were made and their UCL spectra were measured. Generally speaking, the intensity of green emission is high, and the intensity of red emission is relatively weak (Fig. 6). It should be noted that with the increase of Er^{3+} concentration, the green and red emission intensities of the samples decrease gradually. In our case, when the Er^{3+} ion doping concentration is 0.5 mol%, the green and red UCL intensity reached the maximum (Fig. 7(a)). The UCL intensity decreases with the increase of Er^{3+} concentration, which may be due to the decrease of the distance between two adjacent Er^{3+} ions and the increase of the interaction between the two ions when the concentration of Er^{3+} ion is high, which leads to the concentration quenching of Er^{3+} ion and the weakening of UCL intensity. It is also found from Figure 7b that the ratio of green to red emission intensity increases with the increase of Er^{3+} concentration. The main reason is due to the following cross relaxation (CR)

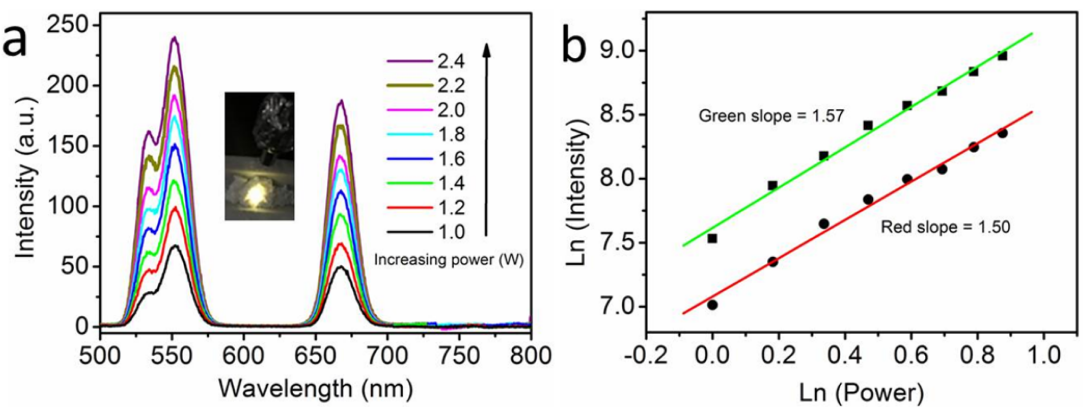

Fig. 4. (a) The UCL spectra and (b) relationship between excitation power and UCL intensity of representative $NaYF_4$: Yb^{3+} 5%, Er^{3+} 0.5% hexagonal nanoplates excited by different laser powers (λ_{ex} = 980 nm). Inset: Digital photo of the UCL phosphors irradiated by infrared laser.

between two adjacent Er^{3+} ions (Fig. 5):

$$CR: Er^{3+}(^4I_{11/2}) + Er^{3+}(^4I_{11/2}) \rightarrow Er^{3+}(^4F_{7/2} + Er^{3+}(^4I_{15/2})$$

With the increase of Er^{3+} doping concentration, the cross relaxation becomes stronger and stronger, resulting in higher green/red emission intensity ratio.

In order to reveal the relationship between the UCL mechanism of $NaYF_4$: Yb^{3+}, Er^{3+} and Yb^{3+} doping concentrations, samples doped with Yb^{3+} concentration (from 0 mol% to 20 mol%) were prepared by controlling the concentration of Er^{3+} at 0.5 mol%. Fig. 8 exhibits the UCL spectra of $NaYF_4$: Yb^{3+} x%, Er^{3+} 0.5% hexagonal nanoplates with different Yb^{3+} ion doping concentrations under 980 nm laser excitation. The UCL intensity of the samples varies greatly by increasing Yb^{3+} doping concentrations (Fig. 8). With the increase of Yb^{3+} concentration, the UCL intensity of the samples gradually increases to the strongest and then decreases, while the ratio of green to red emission intensity decreases all the time (Fig. 9). When the Yb^{3+} ion doping concentration is 5.0 mol%, the intensity of red and green emission is the highest. When the concentration of Yb^{3+} exceeds 5.0%, the UCL of the sample is obviously suppressed. The concentration quenching and reverse energy transfer can be occurred when the concentration of sensitizer is too high. Therefore, there is an optimal concentration of Yb^{3+} in $NaYF_4$: Yb^{3+}, Er^{3+}. Yb^{3+} ions can be doped as sensitizer because the first excited states absorption energy of Yb^{3+} ion and Er^{3+} ion are consistent, and the near-infrared absorption cross section of Yb^{3+} ion is much higher than that of Er^{3+}. Yb^{3+} ions can transfer the energy absorbed by themself to their neighboring Er^{3+} ions. When the doping concentration of Yb^{3+} ions in the sample is high, the energy transfer probability between Yb^{3+} and Er^{3+} will be higher and there will be more electrons in the energy levels of $^4I_{11/2}$ and $^4I_{13/2}$ in Er^{3+} ions. Therefore, with the increase of Yb^{3+} ion concentration, the following CR process will occur [31]:

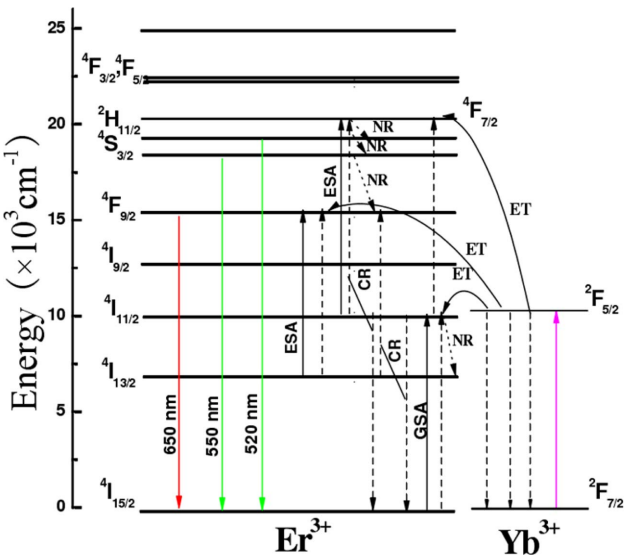

Fig. 5. Energy level diagram of UCL of $NaYF_4$: Yb^{3+}, Er^{3+} phosphors excited by 980 nm laser.

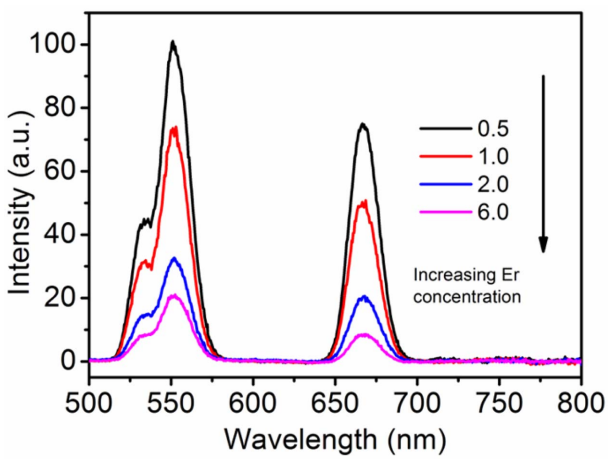

Fig. 6. UCL spectra of $NaYF_4$: Yb^{3+} 10 %, Er^{3+} x% hexagonal nanoplates with different Er^{3+} ion doping concentrations (power = 1.0 W).

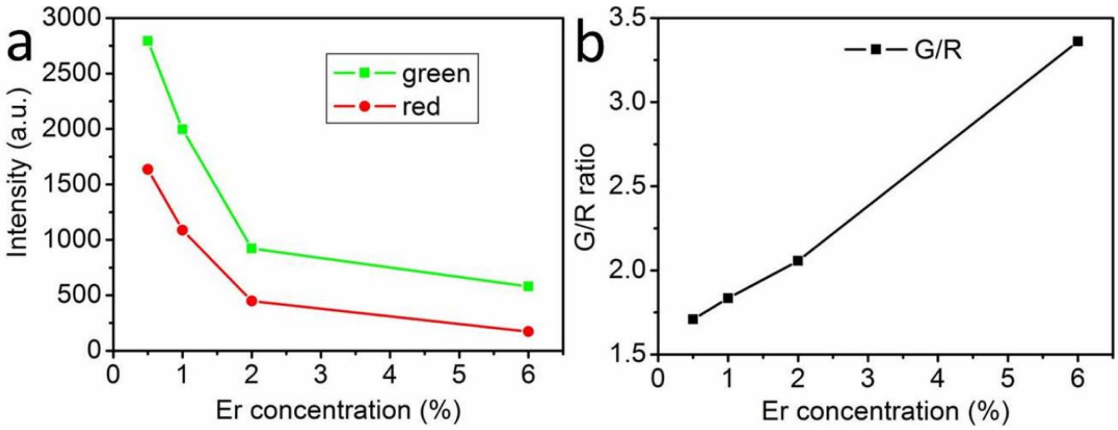

Fig. 7. Emission intensity (a) and green-to-red intensity ratio (b) of the UCL spectra of $NaYF_4$: Yb^{3+} 10 %, Er^{3+} x% hexagonal nanoplates with different Er^{3+} ion doping concentrations (power = 1.0 W).

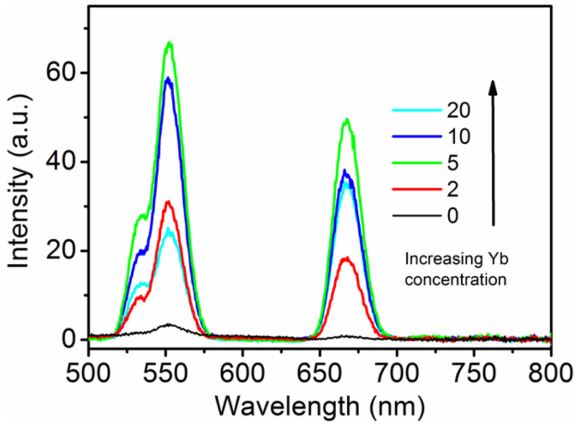

Fig. 8. UCL spectra of $NaYF_4$: Yb^{3+} x %, Er^{3+} 0.5 % hexagonal nanoplates with different Yb^{3+} ion doping concentrations (power = 1.0 W).

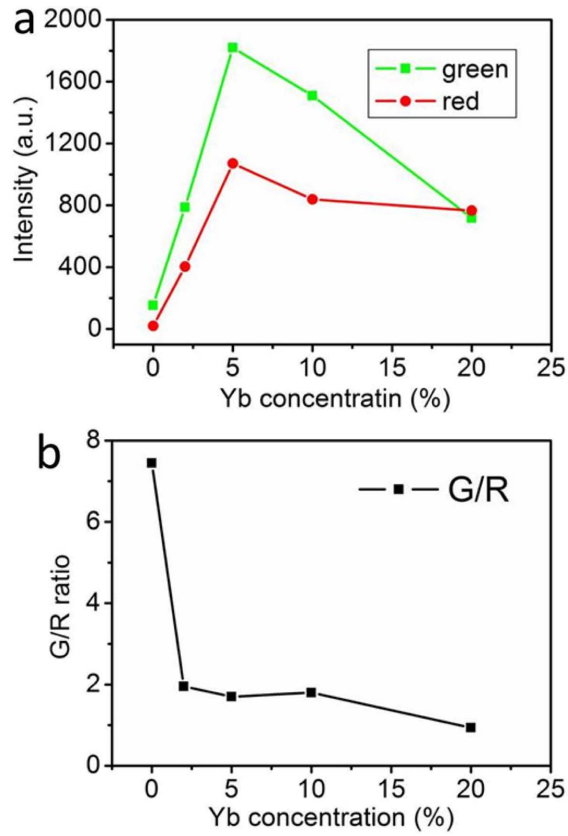

Fig. 9. Emission intensity (a) and green-to-red intensity ratio (b) of the UCL spectra of $NaYF_4$: Yb^{3+} x %, Er^{3+} 0.5 % hexagonal nanoplates with different Yb^{3+} ion doping concentrations (power = 1.0 W).

$$CR: Er^{3+}(^4I_{11/2}) + Er^{3+}(^4I_{13/2}) \rightarrow Er^{3+}(^4F_{9/2}) + Er^{3+}(^4I_{15/2})$$

As a result, the intensity of UCL of red emission becomes stronger.

Summary

$NaYF_4$: Yb^{3+}, Er^{3+} hexagonal nanoplates were synthesized by an IDS Na_4 assisted hydrothermal synthesis method for the first time. Under NIR excitation (980 nm), $NaYF_4$: Yb^{3+}, Er^{3+} hexagonal nanoplates exhibited obviously strong green UCL at 530 and 550 nm and red UCL at 660 nm. The UCL intensity depends on the concentration of Yb^{3+} ion, which acts as a sensitizer ion to improve the absorption around 980 nm, while Er^{3+} acts as an activator ion for UCL in the $NaYF_4$ matrix. The optimum doping concentrations of Er^{3+} and Yb^{3+} for strong UCL luminescence were 0.5 and 5.0 mol%, respectively. The possible CR process in the $NaYF_4$: Yb^{3+}, Er^{3+} hexagonal nanoplates was discussed in detail, which is the main reason for the intensity of UCL related to doping concentration.

Acknowledgements

This work was supported by the Opening Foundation of Henan Key Laboratory of Special Protective Materials (Grant No. SZKFJJ201903).

References

1. F. Auzel, Chem. Rev. 104[1] (2004) 139-174.
2. P. Huang, W. Zheng, S. Zhou, D. Tu, Z. Chen, H. Zhu, R. Li, E. Ma, M. Huang, and X. Chen, Angew. Chem. Int. Ed. 53[5] (2014) 1252-1257.
3. D.K. Chatterjee, M.K. Gnanasammandhan, and Y. Zhang, Small 6[24] (2010) 2781-2795.
4. H.H. Gorris, and O.S. Wolfbeis, Angew. Chem. Int. Ed. 52[13] (2013) 3584-3600.
5. H. Dong, L.D. Sun, and C.H. Yan, Nanoscale 5 (2013) 5703-5714.
6. Z. Gu, L. Yan, G. Tian, S. Li, Z. Chai, and Y. Zhao, Adv. Mater. 25[28] (2013) 3758-3779.
7. Y. Liu, D. Tu, H. Zhu, and X. Chen, Chem. Soc. Rev. 42[16] (2013) 6924-6958.
8. E. Hemmer, N. Venkatachalam, H. Hyodo, A. Hattori, Y. Ebina, H. Kishimoto, and K. Soga, Nanoscale 5[23] (2013) 11339-11361.
9. S. Wang, J. Feng, S. Song, and H. Zhang, CrystEngComm 15[36] (2013) 7142-7151.
10. M. Haase, and H. SchC$fer, Angew. Chem. Int. Ed. 50[26] (2011) 5808-5829.
11. P. Qiu, N. Zhou, H. Chen, C. Zhang, G. Gao, and D. Cui, Nanoscale 5[23] (2013) 11512-11525.
12. Q. Liu, W. Feng, and F. Li, Coordin. Chem. Rev. 273-274 (2014) 100-110.
13. X. Liu, R. Deng, Y. Zhang, Y. Wang, H. Chang, L. Huang, and X. Liu, Chem. Soc. Rev. 44[6] (2015) 1479-1508.
14. L. Tu, X. Liu, F. Wu, and H. Zhang, Chem. Soc. Rev. 44[6] (2015) 1331-1345.
15. J. Zhao, H. Yang, J. Li, Y. Wang, and X. Wang, Sci. Rep-UK. 7 (2017) 18014.
16. J. Zhou, Q. Liu, W. Feng, Y. Sun, and F. Li, Chem. Rev. 115[1] (2015) 395-465.
17. Y. Wang, L. Tu, J. Zhao, Y. Sun, X. Kong, and H. Zhang, J. Phys. Chem. C 113 (2009) 7164-7169.
18. A.S. Oliveira, M.T. De Araujo, A.S. Gouveia-Neto, J.A. Medeiros Neto, A.S.B. Sombra, and Y. Messaddeq, Appl. Phys. Lett. 72[7] (1998) 753-755.

19. C. Strohhöfer, and A. Polman, J. Appl. Phys. 90[9] (2001) 4314-4320.
20. Y. Wang, K. Zheng, S. Song, D. Fan, H. Zhang, and X. Liu, Chem. Soc. Rev. 47[17] (2018) 6473-6485.
21. S.H. Kang, J.H. Ryu, C.W. Park, J.H. Park, H.M. Kim, H.S. Kang, J.S. Choi, J.H. Jung, B.G. Choi, and K.B. Shim, J. Ceram. Process. Res. 17[2] (2016) 118-121.
22. J.H. Ryu, S.H. Kang, and K.B. Shim, J. Ceram. Process. Res. 17[3] (2016) 253-256.
23. S.H. Kang, H. A. Lee, J.H. Park, C.W. Park, H.M. Kim, H.S. Kang, J.S. Choi, J.H. Jung, J. H. Ryu, and K.B. Shim, J. Ceram. Process. Res. 17[5] (2016) 468-471.
24. T. Nunokawa, Y. Onodera, H. Kobayashi, T. Asahi, O. Odawara, and H. Wada, J. Ceram. Process. Res.14[s1] (2013) 1-4.
25. K.W. Krämer, D. Biner, G. Frei, H.U. Güdel, M.P. Hehlen, and S.R. Lüthi, Chem. Mater. 16[7] (2004) 1244-1251.
26. N. Menyuk, K. Dwight, and J.W. Pierce, Appl. Phys. Lett. 21[4] (1972) 159-161.
27. Y. Sun, Y. Chen, L. Tian, Y. Yu, X. Kong, J. Zhao, and H. Zhang, Nanotechnology 18[27] (2007) 275609.
28. J. Zhao, Y. Sun, X. Kong, L. Tian, Y. Wang, L. Tu, J. Zhao, and H. Zhang, J. Phys. Chem. B 112[49] (2008) 15666-15672.
29. J. Zhao, X. Liu, D. Cui, Y. Sun, Y. Yu, Y. Yang, C. Du, Y. Wang, K. Song, K. Liu, S. Lu, X. Kong, and H. Zhang, Eur. J. Inorg. Chem. 2010[12] (2010) 1813-1819.
30. M. Pollnau, D.R. Gamelin, S. R. LüthiL, H.U. Güdel, and M.P. Hehlen, Phys. Rev. B 61[5] (2000) 3337-3346.
31. H.Q. Liu, L.L. Wang, and S. Chen, Mater. Lett. 61[17] (2007) 3629-3631.